

# Raman spectroscopy of multiferroic trigonal boracite $\text{Co}_3\text{B}_7\text{O}_{13}\text{Cl}$

M. N. Iliev and V. G. Hadjiev

*Texas Center for Superconductivity, University of Houston, Texas 77204-5002, USA*

M. E. Mendoza

*Instituto de Física, Universidad Autónoma de Puebla, Apartado Postal J-48, Puebla, Puebla 72570, Mexico*

J. Pascual

*Institut Català de Nanotecnologia (ICN) Edifici CM7, Campus de la UAB, 08193 Bellaterra (Barcelona), Spain and Departament de Física Edifici Cn, Universitat Autònoma de Barcelona, 08193 Bellaterra (Barcelona), Spain*

(Received 27 September 2007; published 20 December 2007)

Raman microscopy was applied to study the polarized Raman scattering from untwinned domains of  $\text{Co}_3\text{B}_7\text{O}_{13}\text{Cl}$  (Co-Cl) in the trigonal,  $R3c$ , ferroelectric phase. The symmetry ( $A_1$  or  $E$ ) and mode polarization (LO or TO) for all observed Raman lines were determined from comparison of the spectra measured in several scattering configurations. It was found that as a rule, the TO-LO splitting is small or negligible. A group of  $A_1$  modes, characterized by a quasi-one-component Raman tensor, was tentatively assigned to stretching vibrations of Cl, O, or B along the trigonal axis, which in this material is parallel to the ferroelectric polarization direction.

DOI: [10.1103/PhysRevB.76.214112](https://doi.org/10.1103/PhysRevB.76.214112)

PACS number(s): 78.30.-j, 77.84.Bw, 64.70.Kb

## I. INTRODUCTION

The boracites with the general formula  $M_3\text{B}_7\text{O}_{13}X$  ( $M$  = divalent metal,  $X = \text{Cl, Br, I}$ ), shortly denoted as  $M$ - $X$ , are among the first known multiferroic materials. The increasing attention to novel physical effects revealed in multiferroics is attracting a renewed interest to the properties of boracites.  $\text{Co}_3\text{B}_7\text{O}_{13}\text{Cl}$  (Co-Cl) is a typical boracite that exhibits a sequence of transitions from the high temperature paraelectric  $F\bar{4}3c$  cubic phase to the ferroelectric orthorhombic  $Pca2_1$  (at 623 K), monoclinic  $Pa$  (at 538 K), trigonal  $R3c$  (at 468 K), and finally to the monoclinic  $Cc$  phase below 9–11 K.<sup>1,2</sup> In the latter phase, both ferroelectric and magnetic orders coexist. Structural, ferroelectric, and magnetic properties of Co-Cl boracite have been reported,<sup>3–5</sup> but there is to our knowledge no report on the lattice dynamics of this material. The few studies on the Raman spectra of boracites have been restricted so far to the cubic and orthorhombic materials<sup>6–10</sup> with only one exception on trigonal boracite—an earlier work of Lockwood<sup>11</sup> where the Raman spectra of  $\text{Zn}_3\text{B}_7\text{O}_{13}\text{Cl}$  (Zn-Cl) have been reported. Due to the twinned structure of Zn-Cl and the use of a macro-Raman setup, however, the reported experimental spectra do not correspond to a single scattering configuration and the tentative assignment of the symmetry of the Raman lines is dubious.

In this work, we present results of a detailed study of polarized Raman spectra of trigonal Co-Cl at room temperature with particular attention to the coexistence of four crystallographically distinct twin variants with orientation of the trigonal axis along the  $[111]_c$ ,  $[\bar{1}\bar{1}\bar{1}]_c$ ,  $[\bar{1}\bar{1}1]_c$ , and  $[1\bar{1}\bar{1}]_c$  directions of the parent cubic phase. After visualizing these twin variants by Raman imaging of their projections on the pseudocubic  $(100)_c$ ,  $(110)_c$ ,  $(111)_c$ , and  $(112)_c$  surfaces, we were able to obtain spectra from untwinned domains in several exact scattering configurations, including those where either pure TO or pure LO modes are pronounced. In addition

to the classification of modes by symmetry, we discuss the one-dimensional character of some of the  $A_1$  modes, as well as the negligible LO-TO splitting for the most  $A_1$  and  $E$  modes.

## II. SAMPLES AND EXPERIMENT

Co-Cl boracite single crystals were grown by chemical vapor transport method.<sup>12,13</sup> The as-grown crystals exhibit  $(100)_c$ ,  $(111)_c$ , and  $(110)_c$  facets (in cubic notation), the largest being of  $(100)_c$  type and the smallest ones of  $(110)_c$  type. The Raman spectra were measured under a microscope ( $50\times$  magnification) using a T64000 Horiba JY triple spectrometer with 633 nm excitation. The diameter of the laser spot was 2–3  $\mu\text{m}$  and the incident laser power was kept below 5 mW. To assure that the Raman signal is obtained from a single untwinned domain, we used an  $XY$  motorized stage for Raman mapping of areas of up to  $90\times 180\ \mu\text{m}^2$  size at 1.5  $\mu\text{m}$  steps on as-grown  $(100)_c$ ,  $(111)_c$ , and  $(110)_c$  or freshly broken surface containing the  $[111]_c$  cubic direction. On all these surfaces, the Raman mapping revealed untwinned mostly stripe-shaped domains of width up to 10  $\mu\text{m}$ , which could be used for obtaining polarized Raman spectra in exact scattering geometry. The direction of the trigonal axis in these domains has been determined accounting that it is along one of the  $\langle 111 \rangle_c$  direction and taking use of the finding (see Sec. III) that several  $A_1$  modes have a maximum (minimum) intensity for incident light polarization parallel (perpendicular) to the projection of the trigonal axis on the surface. Figure 1 displays the optical image of an area on the  $(110)_c$  surface and the corresponding Raman image of the scattering intensity distribution for the  $150\ \text{cm}^{-1}$  mode, as obtained with incident ( $\vec{e}_i$ ) and scattered ( $\vec{e}_s$ ) light polarizations parallel to  $[110]_c$ . The red (dark) stripes in Fig. 2(b) correspond to the  $[111]_c$  and  $[\bar{1}\bar{1}\bar{1}]_c$  twin variants with pro-

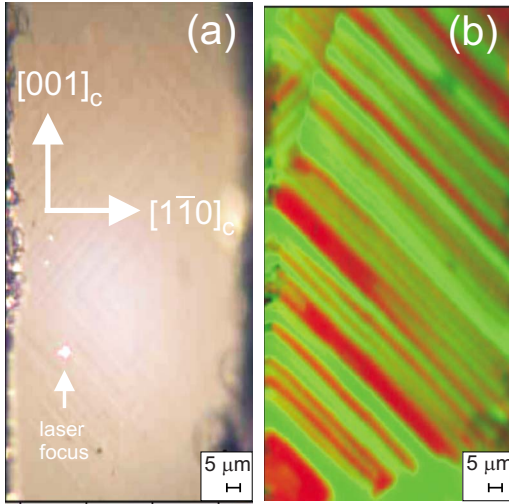


FIG. 1. (Color online) (a) Optical image of a part of  $(110)_c$  pseudocubic surface. (b) Intensity distribution of the  $150 \text{ cm}^{-1}$  Raman peak over the same area measured with parallel scattering configuration,  $\vec{e}_i \parallel \vec{e}_s \parallel [1\bar{1}0]_c$ , with  $1.5 \mu\text{m}$  resolution. Red (dark) and green (bright) colors denote weak and strong  $150 \text{ cm}^{-1}$  mode intensities, respectively.

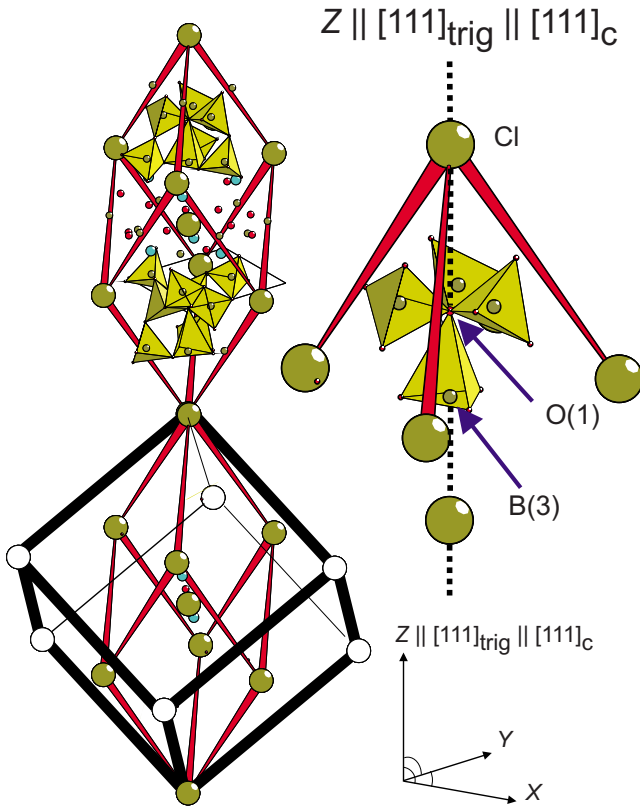


FIG. 2. (Color online) Trigonal primitive cell of  $\text{Co}_3\text{B}_7\text{O}_{13}\text{Cl}$  and the face-centered elementary cell of the parent cubic structure. A fragment of the structure illustrating the positions of Cl, B(3), and O(1) atoms on the trigonal axis and the  $XYZ$  orthogonal coordinate system of the Raman tensors are also shown.

TABLE I. Wyckoff positions and irreducible representations ( $\Gamma$ -point phonon modes) for  $\text{Co}_3\text{B}_7\text{O}_{13}\text{Cl}$  (space group  $R3c$ , No. 161,  $Z=2$ ). The Raman tensors are given in orthogonal system with  $Z$  direction parallel to  $[111]_{\text{trig}} \equiv [111]_{\text{cubic}}$ .

Atom	Wyckoff position	$\Gamma$ -point phonon modes
Co	$6b$	$3A_1+3A_2+6E$
B(1)	$6b$	$3A_1+3A_2+6E$
B(2)	$6b$	$3A_1+3A_2+6E$
B(3)	$2a$	$A_1+A_2+2E$
O(1)	$2a$	$A_1+A_2+2E$
O(21)	$6b$	$3A_1+3A_2+6E$
O(22)	$6b$	$3A_1+3A_2+6E$
O(23)	$6b$	$3A_1+3A_2+6E$
O(24)	$6b$	$3A_1+3A_2+6E$
Cl	$2a$	$A_1+A_2+2E$

Mode classification  
 $\Gamma_{\text{Raman}} = 23A_1 + 47E$   
 $\Gamma_{\text{IR}} = 23A_1 + 47E$   
 $\Gamma_{\text{acoustic}} = A_1 + E$   
 $\Gamma_{\text{silent}} = 24A_2$

$$A_1(z) \rightarrow \begin{bmatrix} a & 0 & 0 \\ 0 & a & 0 \\ 0 & 0 & b \end{bmatrix} \quad E(x), E(y) \rightarrow \begin{bmatrix} c & 0 & d \\ 0 & -c & 0 \\ d & 0 & 0 \end{bmatrix}, \begin{bmatrix} 0 & -c & 0 \\ -c & 0 & d \\ 0 & d & 0 \end{bmatrix}$$

jections of the trigonal axis along  $[001]_c$ . The green-colored parts of Fig. 1(b) are the twin variants with  $[\bar{1}11]_c$  and  $[1\bar{1}1]_c$  orientations of the trigonal axes.

To avoid confusion about the notations for the pseudocubic structure and trigonal domains, further in the text, the standard  $(hkl)_c$  and  $[hkl]_c$  notations will be used, respectively, for the surfaces and directions of the pseudocubic structure. The directions in a particular trigonal twin variant and related Raman scattering configurations are given in Cartesian  $XYZ$  coordinate system, where  $Z$  is parallel to the direction of the threefold trigonal axis  $[111]_{\text{trig}} \equiv [111]_c$  and  $X$  and  $Y$  are two orthogonal direction perpendicular to  $Z$ .

### III. $\Gamma$ -POINT PHONONS IN TRIGONAL BORACITES

The primitive trigonal cell of boracites, shown in Fig. 2, contains 2 f.u. with all atoms in noncentrosymmetrical positions. The classification of the  $\Gamma$ -point phonon modes is given in Table I.

Given that the crystallographic directions are known, the symmetry of Raman modes as well as the relative value of nonzero components of the corresponding Raman tensors can be determined by comparing the Raman spectra measured in several exact scattering configurations, such as  $X(ZZ)\bar{X}$ ,  $X(YY)\bar{X}$ ,  $X(ZY)\bar{X}$ ,  $Z(XX)\bar{Z}$ , and  $Z(XY)\bar{Z}$ .<sup>14</sup> As we are dealing with polar vibrations in a uniaxial crystal, depending on the angle  $\theta$  between the directions of the phonon wave vector  $\vec{q}$  and atomic motions of the  $A_1$  and  $E$  modes (along  $Z$

TABLE II. Intensities of the  $A_1$  and  $E$  modes with different scattering configurations.  $X$ ,  $Y$ , and  $Z \parallel [111]_c \parallel [111]_{trig}$  are unit vectors along the direction of Cartesian coordinate system of the Raman tensors.  $Y' \parallel Y+Z$ ,  $Z' \parallel Y-Z$ . The notations TO and LO are correct under the assumption that the atomic motions of the  $A_1$  modes are along the  $Z$  direction and those of the  $E$  modes are in the  $XY$  plane, which may be not the case for some modes.

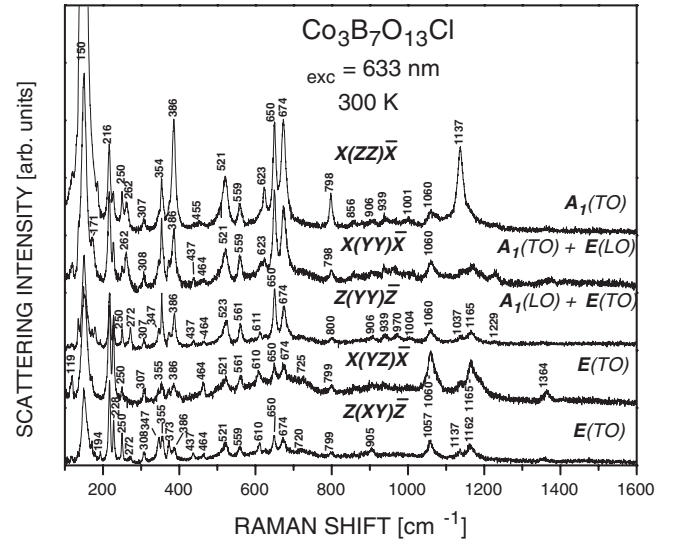
Cubic crystal surface	Scattering configuration	Intensity			
		$A_1$ (TO)	$A_1$ (LO)	$E$ (TO)	$E$ (LO)
$(112)_c$	$X(ZZ)\bar{X}$	$b^2$			
$(112)_c$	$X(ZY)\bar{X}$			$d^2$	
$(112)_c$	$X(YY)\bar{X}$	$a^2$			$c^2$
$(112)_c$	$X(Y'Y')\bar{X}$	$\frac{1}{4}(a+b)^2$		$d^2$	$\frac{1}{4}c^2$
$(112)_c$	$X(Y'Z')\bar{X}$	$\frac{1}{4}(a-b)^2$			$\frac{1}{4}c^2$
$(111)_c$	$Z(YY)\bar{Z}$		$a^2$	$c^2$	
$(111)_c$	$Z(XY)\bar{Z}$			$c^2$	

or perpendicular to  $Z$ ), we observe either pure LO and TO modes or mixture of LO and TO modes. For a backscattering configuration,  $\vec{q}$  is parallel to the direction of incident light and the simplest cases are  $\theta=0^\circ$  (LO) and  $\theta=90^\circ$  (TO). Mode polarizations and intensities for the scattering geometries used in our experiments are summarized in Table II. It is worth noting that for a given mode, the nonzero elements of the Raman tensor may be significantly different for the TO and LO components.

#### IV. RESULTS AND DISCUSSION

Figure 3 shows the polarized Raman spectra of Co-Cl as obtained from single twin variants with known orientation. The phonon frequencies are summarized in Table III. A comparison of the spectra leads to following findings: (i) most of the  $A_1$  modes have an  $E$  mode partner with practically the same frequency; (ii) as a rule, the LO-TO splitting, if observable, is small; (iii) several  $A_1$  modes, in particular, those at 150, 623, 798, and 1137  $\text{cm}^{-1}$ , are much stronger with  $ZZ$  than  $XX$  polarization.

Looking for explanation of these findings, one turns to the correlation between the normal modes in trigonal and cubic phases of Co-Cl, which have primitive unit cells of the same volume.<sup>11</sup> A factor group analysis of the 144-dimensional  $\Gamma$ -point reducible representation gives the symmetry reduction  $\Gamma_{144}^c = 4A_1 + 6A_2 + 10E + 18F_1 + 20F_2$  for the cubic phase, which becomes  $\Gamma_{144}^t = 4A_1 + 6A_2 + 10E + 18(A_2 + E) + 20(A_1 + E)$  in the trigonal phase. It is plausible to assume that due to the weak trigonal distortion, the trigonal  $A_1$  and  $E$  modes, originating from a given cubic  $F_2$  mode, will be very close in frequency, as experimentally observed. At this stage, however, we cannot explain the lack of pronounced LO-TO splitting for these modes, having in mind that the parent cubic  $F_2$  modes are also polar ones.



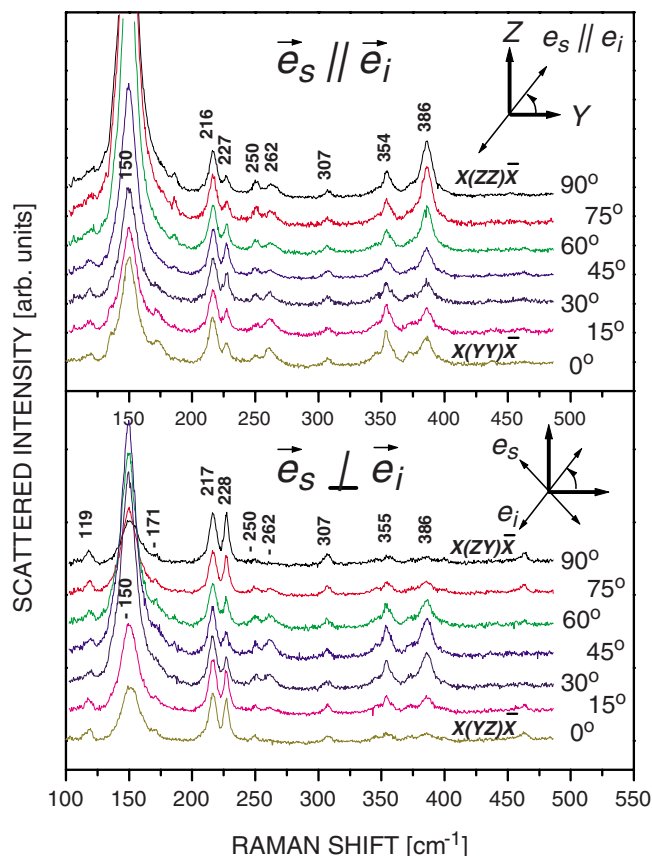


FIG. 4. (Color online) Angular dependence of the low frequency part of the Raman spectra of  $\text{Co}_3\text{B}_7\text{O}_{13}\text{Cl}$  as obtained from the  $YZ$  surface with 633 nm excitation with parallel and crossed scattering configurations.

vector that is perpendicular to  $\vec{e}_i$  is represented as  $(-\sin \varphi, 0, \cos \varphi)$ . The Raman intensity is given by  $I(\varphi) \propto [\vec{e}_s \mathbf{R} \vec{e}_i]^2$ , where  $\vec{e}_s$  is the scattered light polarization. For an  $A_1$  mode,  $I(\varphi)$  takes the form  $I^{\parallel}(\varphi) \propto [a \cos^2 \varphi + b \sin^2 \varphi]^2$  and  $I^{\perp}(\varphi) \propto [(b-a)^2 \sin^2 \varphi \cos^2 \varphi]$  for parallel  $\vec{e}_i \parallel \vec{e}_s$  and crossed  $\vec{e}_i \perp \vec{e}_s$  polarization, respectively. The scattering configurations  $X(YY)\bar{X}$  and  $X(YZ)\bar{X}$  correspond to  $\varphi=0^\circ$ , whereas  $X(ZZ)\bar{X}$  and  $X(ZY)\bar{X}$  correspond to  $\varphi=90^\circ$ .

The angular dependence of Raman intensity in the low frequency spectra containing the  $150 \text{ cm}^{-1}$  mode is illustrated in more detail in Fig. 4. These spectra were obtained from a  $YZ$  surface by its rotation around  $X$  at fixed incident polarization. Due to a small misalignment, the Raman peaks do not reach their maximum or minimum values observed for the spectra in Fig. 3, but the type of intensity variations is obvious. In parallel configuration, the  $A_1$  peak at  $150 \text{ cm}^{-1}$  increases significantly from  $\varphi=0^\circ$  to  $\varphi=90^\circ$ . In the cross polarized spectra, its intensity has minima for  $\varphi=0^\circ$  and  $\varphi=90^\circ$  but reaches a relative maximum at  $\varphi=45^\circ$ . Such variations evidence that for the  $150 \text{ cm}^{-1}$  mode, the relation  $b \gg a$  is satisfied. Although less dramatic, the intensity variations for the  $385 \text{ cm}^{-1}$  peak are similar, indicating that in this case the inequality  $b > a$  is valid. The opposite relation  $b < a$  is consistent with the variations of the  $354 \text{ cm}^{-1}$  mode.

The strong inequality  $b \gg a$ , most clearly pronounced for the  $150, 623, 798,$  and  $1137 \text{ cm}^{-1}$   $A_1$  modes, is typical for pure stretching modes, where, as a rule, the Raman intensity with parallel polarization is high along the stretching direction and much lower perpendicular to it. An attempt to identify the pure stretching modes starts with the identification of atoms bonded to their neighbors along this direction. As it follows from Fig. 2, such atoms are Cl, B(3), and O(1).

The lightest of these atoms is B(3) and it is plausible to assign the  $1137 \text{ cm}^{-1}$  mode to B(3) vibrations between O(1) and Cl. The  $623$  and  $798 \text{ cm}^{-1}$  modes have frequencies typical for oxygen stretching vibrations. The fact that there are two modes with similar polarization properties indicates that, except for O(1) stretch against B(3), motions of other atoms could be involved in these modes. Most intriguing is the origin of the  $150 \text{ cm}^{-1}$  mode. Based on its lower frequency and stretching features, it has to be assigned to vibrations of heavier atoms, either Co or Cl. Co atoms, however, have no bonds parallel to  $Z$ . Moreover, if Co vibrations are responsible for the  $150 \text{ cm}^{-1}$  mode, the corresponding mode in the isostructural Zn-Cl should be observed at lower frequency. This is not the case as in Zn-Cl, this peak shifts in opposite direction to  $156 \text{ cm}^{-1}$ .<sup>11</sup> Therefore, we have strong arguments to assign the  $150 \text{ cm}^{-1}$  mode to stretching vibrations of Cl. The low frequency of this mode is consistent with both low charge of  $\text{Cl}^-$  and long Cl-B(3) bond.<sup>5</sup>

The results of this work may become the starting point of a more profound study of structure-property relationships in multiferroic boracites. We expect that the Raman imaging microscopy could visualize the evolution of domain structure from the paraelectric cubic phase through all structural transitions down to the magnetic ordered phase(s). It is also plausible to expect that the variation of Raman spectra through these transitions will help in Raman line assignment and will provide valuable information on the coupling between lattice, magnetic, and ferroelectric orders.

## V. CONCLUSIONS

In conclusion, Raman microscopy has successfully been applied to resolve the multidomain structure of trigonal boracite  $\text{Co}_3\text{B}_7\text{O}_{13}\text{Cl}$  and obtain the Raman spectra in exact scattering configurations. The symmetry of all observed Raman lines has been determined. The close coincidence of  $A_1$  and  $E$  mode frequencies and small LO-TO splitting have been related to the closeness of trigonal and cubic structures. Four of the most pronounced  $A_1$  modes have tentatively been assigned to stretching vibrations of Cl, B(3), and O(1) along the trigonal axis.

## ACKNOWLEDGMENTS

This work was supported in part by the State of Texas through the Texas Center for Superconductivity at the University of Houston (TcSUH). M.E.M. acknowledges the financial support of Secretaria de Estado de Universidades e Investigacion de Espana under the Grant No. SAP 2005-0132.

- <sup>1</sup>R. J. Nelves, *J. Phys. C* **7**, 3840 (1974).
- <sup>2</sup>P. Toledano, H. Schmid, M. Clin, and J. P. Rivera, *Phys. Rev. B* **32**, 6006 (1985).
- <sup>3</sup>M. S. Kumar, J. P. Rivera, Z. G. Ye, S. D. Gentil, and H. Schmid, *Ferroelectrics* **204**, 57 (1997).
- <sup>4</sup>G. Quézel and H. Schmid, *Solid State Commun.* **6**, 447 (1968).
- <sup>5</sup>J. Ju, H. M. Li, Y. X. Wang, J. H. Lin, and C. Dong, *J. Mater. Chem.* **12**, 1771 (2002).
- <sup>6</sup>D. J. Lockwood, *J. Raman Spectrosc.* **2**, 555 (1974).
- <sup>7</sup>D. J. Lockwood, *Solid State Commun.* **18**, 115 (1976).
- <sup>8</sup>A. F. Murray and D. J. Lockwood, *J. Phys. C* **11**, 2349 (1978).
- <sup>9</sup>A. F. Murray and D. J. Lockwood, *J. Phys. C* **11**, 4651 (1978).
- <sup>10</sup>D. J. Lockwood, *Indian J. Pure Appl. Phys.* **16**, 268 (1978).
- <sup>11</sup>D. J. Lockwood, *Ferroelectrics* **29**, 19 (1980).
- <sup>12</sup>H. Schmid, *J. Phys. Chem. Solids* **26**, 1973 (1965).
- <sup>13</sup>H. Schmid, *Phys. Status Solidi* **37**, 209 (1970).
- <sup>14</sup>The first and fourth letters in these notations denote the propagation directions of incident and scattered light, respectively. The second and third letters denote, respectively, incident and scattered polarization directions.